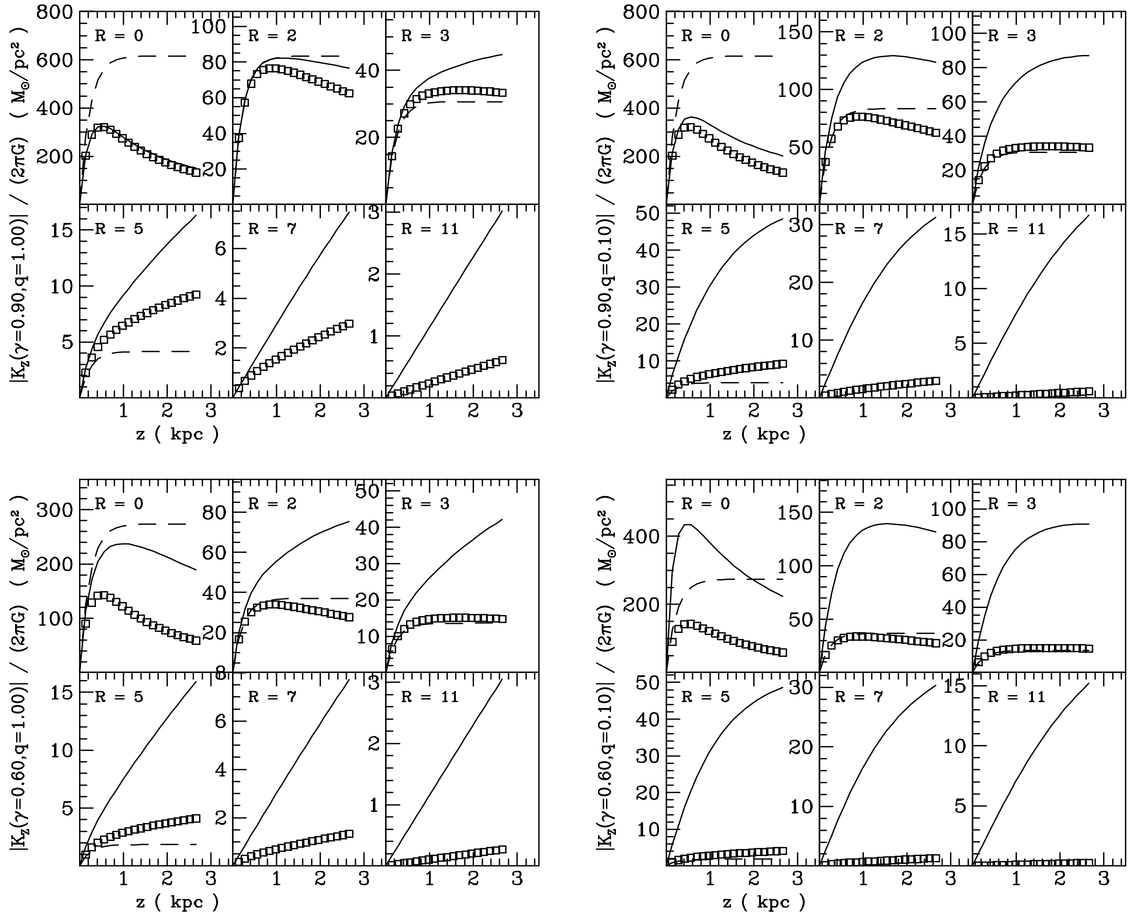

Fig. 6.— In this collage of model galaxies, each plot represents the vertical force, $K_z(z;\gamma,q)$, as a function of height above the plane (z). The top plots correspond to a γ=0.9-disk, the lower two plots to a γ=0.6-disk. The left-hand side plots were calculated for a round ($q = 1.0$) halos; the two right most plots for a flat ($q = 0.1$) halos. The different panels inside each plot correspond to different radii (in units of h_{R}). All panels have been calculated for a galaxy model consistent with the observed properties of NGC 3198 (BE89). The open squares represent the vertical force due to a double exponential stellar disk. The dashed line is the vertical force valid for the local approximation. The full line is the sum of the vertical force from the stellar disk and DM halo. We notice that the maximum-disk plus round DM halo combination is the only region in γ, q-space where the stellar disk is dominant over the entire extent of the stellar disk ($R \lesssim 5h_{\mathrm{R}}$). For this combination of γ and q, the stellar disk contributes significantly ($\approx$ 20 % at 11 h_{R}) to the vertical force, even beyond the truncation of the stellar disk (at $6h_{\mathrm{R}}$). Furthermore notice, that the *shapes* of the vertical forces generated by a very flattened DM halo are very similar to the *shapes* of the vertical force in a round DM halo, but that the *amplitudes* are about twice larger.

2.3.4. The plane-parallel-sheet case

The difference between the plane-parallel-sheet case and the global approach is most easily illustrated by plotting the vertical forces for the two cases. In Fig. 6 I plot the $K_{\mathrm{z}}(z)$ forces, as calculated for a NGC 3198-model, for a selection of radii. The dashed line is the vertical force due to a plane parallel sheet of stars with an exponential vertical distribution and a column density appropriate for the indicated radius. The open squares represent the force generated by a radially truncated exponential disk. The full line represents the $K_{\mathrm{z}}(z)$ generated by the combined density distribution of the stellar disk and the DM halo. For the combination of parameters, maximum-disk and round DM halo (top-left panel), the plane-parallel-sheet case overestimates the vertical force in the inner two scale-lengths of the stellar disk, because the plane parallel sheet is a bad approximation to the fast radially declining surface density (there is very little surface area at the central surface density). Furthermore, the large negative ρ_{rot} associated with the steeply rising rotation curve (Fig. 4) decreases the effective volume density. Beyond about 2 h_R the potential due to the interior stellar disk becomes more important and will eventually dominate the potential generated by the local column of stars. Additional model calculations (top-right panel: $\gamma = 0.9, q = 0.1$; bottom-left panel: $\gamma = 0.6, q = 1.0$; bottom-right panel: $\gamma = 0.6, q = 0.1$) show that the stellar disk has a dominating contribution to the vertical force (over the extent of the stellar disk) if and only if the stellar disk is close to "maximum" and if the DM halo is close to round (see also Sec. 2.6.4. and Fig. 14).

2.3.5. Inferences

From the Figs. 5, 6 and 7 we learn the following:
—At large galactocentric radii ($R \geq 6h_R$), K_{z} is almost linear for the range of models considered here, resulting in an almost Gaussian vertical distribution for the gas. Notwithstanding the low stellar surface densities at these large distances, the contribution of the stellar disk to the total vertical force can be substantial: even at eleven radial scale-lengths the stellar disk contributes about 20 % of the total vertical force (for the round DM halo cases). The self-gravity of the gas (see Fig. 7), which is discussed in more detail in Sec. 2.3.6., can be important (up to 50% of the total force) in this region as well.
—In the transition region ($4h_R \leq R \leq 6h_R$) the contribution of the stellar disk, the gaseous disks, and the dark halo to the total vertical force can be of comparable magnitude (for the mass model with maximum disk, round halo, and typical gaseous surface densities. See Fig. 7). Stellar disks are truncated (vdKS81a&b; vdKS82a&b; BD93) causing a sharp discontinuity in the stellar densities. However the potential as generated by the total stellar mass distribution will change much less abruptly. Thus the local approaches will strongly overpredict the thickness of the gas layer in this region (see Fig. 5). Moving away from this corner ($\gamma = 0.9, q = 1.0$) in parameter space increases the halo's contribution to the total potential significantly.

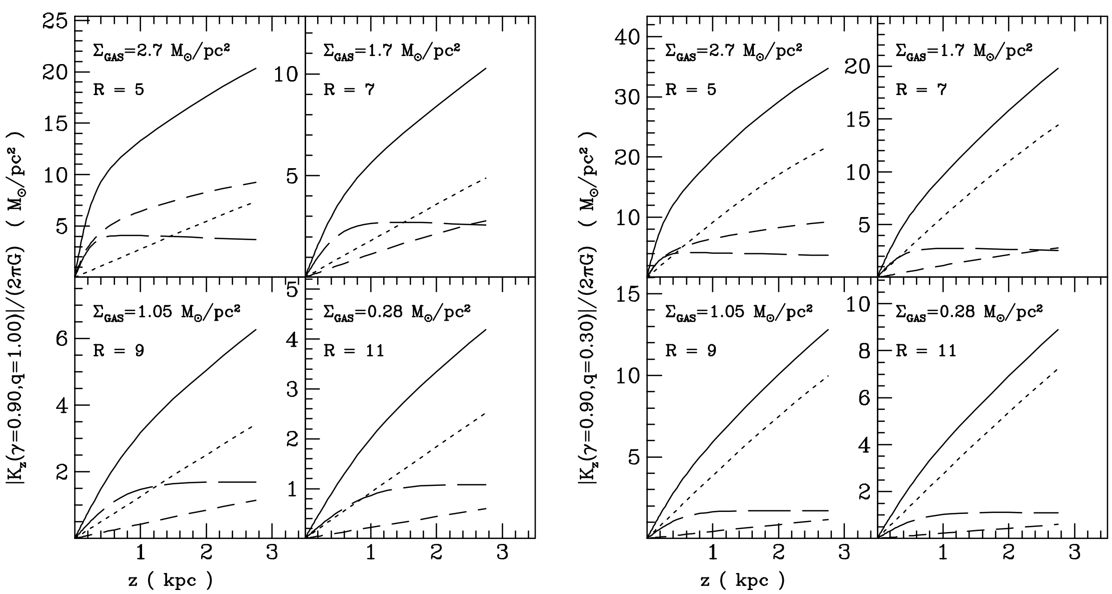

Fig. 7.— This figure presents the vertical force in the region beyond the optical disk. Again, the galaxy model used, stars+DM-halo+gas, is consistent with the observed properties of NGC 3198 (BE89). The full line is the sum of the vertical force due to the stellar disk, the DM halo and the gas layer. The dotted lines represent the $K_z(z)$ due to the flattened DM halo only ($q = 1.0$ and 0.3 for the Figs. 7a (left-hand plot) and 7b (plot on the right-hand side) respectively). The vertical force arising due to the (truncated) stellar disk is represented by the short dashed line. The long dashed line represents the self-gravity of the gas, whose contribution to the total vertical force can be rather important (30-40%) beyond the optical disk.

—Inside the optical disk, the potential is dominated by the stellar disk only in case the disk is close to "maximum" and the halo is almost round. For the other extreme case (minimum-disk+flat-halo), the potential is completely dominated by the DM halo. In the two remaining corners of parameter space, stellar disk and DM halo contribute about equally to K_z. In all of these cases, the density distribution of a tracer population will be almost Gaussian as long as the velocity dispersion of the tracer is so low that most of the tracer resides at z-heights below the "knee" in K_z (at two to three stellar scale-heights). For a tracer population like the atomic gas with a velocity dispersion of roughly 7 km s^{-1}, the entire extent of the optical disk falls in this regime (see Fig. 10). Isothermal tracers with a velocity dispersion larger than two or three times $\sigma_{z,gas}$ can move beyond the knee in the K_z curve so that their density distribution can no longer be adequately described by a single "simple" function (cf. the thick disk of the Milky Way [e.g. Gilmore & Reid 1983]).
—As expected, both the amplitude and the shape of the vertical force are almost independent of the γ value of the stellar disk if the DM halo is highly flattened. In case of a round DM halo, different γ values for the stellar disk do result in different shapes for the K_z curves.

As the amplitude of the knee in K_z depends linearly on central surface density [quadratically on $V_{rot,max}$, Eqn. (24)], the thickness of the gas layer will be smaller in high rotation curve galaxies and larger in dwarfs (see also Appendix 2.8.).

Two radial regimes are poorly modeled by the Gaussian-equivalent as well as the plane-parallel-sheet local approaches: the region where the rotation curve rises so sharply that ($\rho_{rot} + \rho_{DM} < 0$), and the region where the stellar disk truncates. Special treatment of these regions can be avoided by using the global approach. For those regions where the rotation curve is almost flat, which are far away from the truncation of the stellar disk, the Gaussian-equivalent method works reasonably well.

2.3.6. The Self-Gravity of the Gas

Rupen (1991) finds in NGC 891 as well as in NGC 4565, that the H I volume densities become comparable to the stellar volume densities beyond about 2 radial scale-lengths. For the Milky Way this is true at the solar circle. The self-consistent solution for the multi-component method as found in Appendix 2.6.4. [Eqn. (42)] indicates that the importance of the self-gravity of the gas scales with the ratio of gaseous to stellar kinetic energy. At the solar circle this ratio is about 0.1-0.2, so that the self-gravity of the gas is expected to become increasingly important at larger radii.

The importance of the self-gravity of the gas is illustrated in Fig. 7, where I plot the K_z due to the total (stars+DM+gas) potential (the full line), and the forces arising from the global DM, stellar and gaseous density distributions (dotted, short dashed, and long dashed lines respectively). The self-gravity of the gas has been calculated using the procedure outlined in Sec. 2.3.1..

2.3.7. The multi-component method

In case $\rho_{\rm rot}$ and the self-gravity of the gas are neglected it is rather straightforward to show (van der Kruit, 1988) that different isothermal components subject to the same cylindrically symmetric gravitational field have vertical distributions which are powers of each other. Including $\rho_{\rm rot}$, the self-gravity of the gas, and the dark matter halo leads to the multi-component method, first used by Bahcall (1984) to determine the amount of disk-like dark matter in the solar neighborhood. In Appendix 2.7., I present an analytic solution [Eqn. (42), which needs to be solved iteratively] to Eqn. (12). In the same Appendix I also show that in the multi-component method the distribution of the gas is a power of the distribution of the stars as well. In Fig. 9 I compare the model widths calculated in the multi-component method (where the vertical distribution of the stellar disk is fixed to a sech-squared , see Appendix 2.7.) with those calculated using the global approach. The top plot shows the percentage difference between the global and local approaches. The structure in these difference curves mostly arrises due to small scale structure in the observed rotation curve. Thus, application of the multi-component method could be misleading. For example, if the flaring measurements extend to a radius at which the local approach predicts a local maximum in the observable width, too round a DM halo would be inferred.

I used the multi-component method to compare models of NGC 3918 with a varying amount of gaseous self-gravity. The results are presented in Fig. 8. In the left-hand set of panels I show the width, W_{gas} [$\approx FWHM/2.35$, as defined by Eq. (5)], of the gas layer as a function of galactocentric radius for three different halo flattenings (bottom panel, $q = 1.0$; middle panel, $q = 0.5$; upper panel, $q = 0.1$). Four different curves are presented, the different lines corresponds to differently scaled gaseous surface densities: 1/100, 1, 5, and 10 times the measured surface density for the full line, the dotted line, the short dashed line and the long dashed line respectively. The models are calculated[10] for a gaseous velocity dispersion of 7.5 km s^{-1} and a stellar disk with a γ value of 0.93 (i.e. about maximum-disk). For the scaled gaseous disks I plot (right-hand set of panels) the ratio of thickness of the scaled disk and the thickness of the no-self-gravity-disk. From this plot we see that not including the gaseous self-gravity will result in an *overestimate* of the width of the gas layer (by approximately 10% to 20%).

[10] The effect of the scaling of the gaseous surface density has been taken into account while performing the disk-halo decomposition.

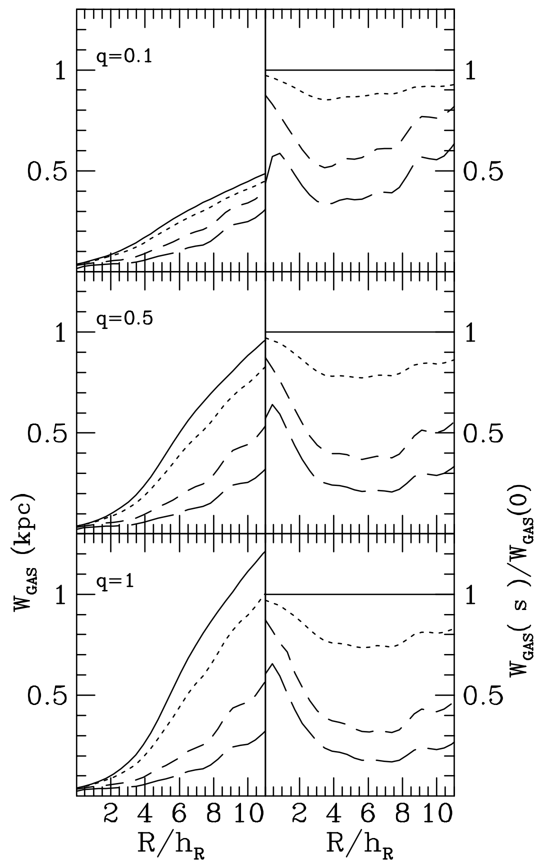

Fig. 8.— In this figure I illustrate the dependence of the thickness of the gas-layer, W_{gas} [$\approx FWHM/2.35$, as defined by Eq. (5)], upon it's self-gravity. I used the multi-component approximation discussed in Appendix 2.7. to calculate NGC 3198-like mass models with varying amounts of gas. For the mass models with the differently scaled gaseous surface densities I performed a separate disk-halo decomposition, all yielding similarly acceptable fits to the observed rotation curve. The left-hand set of panels shows (for $q = 0.1$, $q = 0.5$, and $q = 1$ from top to bottom) the flaring of the gas-layer for several gas-surface-density scaling factors. The scale factor, s, is defined such that $\Sigma_{\rm gas,Model} = s\Sigma_{\rm gas,observed}$; full line , $s = 0.01$; dotted line , $s = 1$; short dashed line , $s = 5$; long dashed line , $s = 10$. In the right-hand set of panels I plot the thickness ratio of scaled surface density to the zero surface density case. From these plots it is clear that the effects of the self-gravity are moderate, but vary systematically with radius for the observed gaseous surface densities. For the upwardly scaled surface densities I find almost no dependence of the gas-layer width on the halo flattening.

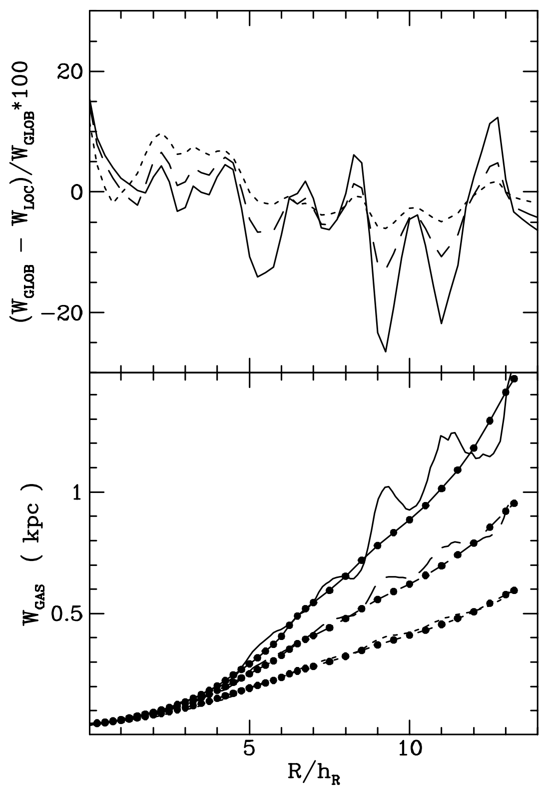

Fig. 9.— In the bottom panel I compare the thickness of the gas layer, W_{gas} [$\approx FWHM/2.35$, as defined by Eq. (5)], as calculated in the global approach (the lines with the filled circles) with the thickness as calculated from the multi-component approach (the lines). For both approaches a fixed $\mathrm{sech}^2(z/(2z_e))$ stellar distribution, truncated at R/h_R=6, was used. Three different DM-halo flattenings are shown (from top to bottom: $q = 1.0$, full line; $q = 0.3$, dashed line; $q = 0.1$, dotted line). In the top panel I plot the percentage difference between the two approaches. The difference between the global and multi-component method mainly arrises due to small scale structure in the observed rotation curve, which has been used to calculate ρ_{rot}.

For the predicted gas-layer width to equal the observed widths a more massive DM halo is required [Eqn. (23)], so that neglecting the self-gravity of the gas will result [using Eqn. (14)] in a *smaller* value (by approximately 20% to 40%) for the halo flattening, q. Thus, in the local approach as well as in the global approach (see Fig. 10), the self-gravity of the gas is found to have a comparable effect on the inferred DM halo flattening.

From these plots I also conclude that for galaxies with relatively large gaseous surface densities the thickness of the gas-layer is not sensitive to the flattening of the dark matter at all. Thus, the self-gravity of the gas may be an unimportant or a significant contributor to the vertical force (for early and late type systems respectively).

2.3.8. Halo shape and gas layer thickness

In order to investigate the dependence of thickness of the gas layer upon the flattening of the DM halo and the $M/\mathcal{L}$ ratio of the stellar disk, I determined $\rho_{\rm gas}(R,z)$ (and $W_{\rm gas}(R)$ therefrom) for a range of galaxy models.

In Fig. 10 I plot the width, W_{gas} [$\approx FWHM/2.35$, as defined by Eq. (5)], of the gas layer in a $\gamma = 0.9$ (i.e. $\sim$ maximum-disk) disk-halo combination for several halo flattenings. The left-hand panel was calculated for a double exponential disk. In the middle panel I incorporated the truncation of the stellar disk (at $R/h_R = 6$), while the self-gravity of the gas is included in the right-hand panel. The effect of the self-gravity of the gas is different for the different disk-halo models, and is strongest between 4 and 8 radial scale-lengths : between 20% and 40% for the NGC 3198 models. Beyond several radial scale-lengths the width of the gas layer depends strongly (roughly proportional to $\sqrt{q}$) on the flattening of the DM halo. Inside the stellar disk, the width of the gas layer is largely independent of the DM-halo flattening because the potential there is dominated by the stellar disk. However, for models with flatter halos and/or lower-γ stellar disks, the halo can be of importance inside the stellar disk (see Sec. 2.3.7., and Fig. 6). It is important to keep in mind that the self-gravity of the gas is more important for the rounder DM-halo models (Sec. 2.3.6. and compare the Figs. 7-a and 7-b). So the "signature" of the halo flattening is somewhat reduced if the self-gravity of the gas is important (see also Fig. 8).

Is the thickness of the gaseous layer dependent on the mass-to-light ratio of the disk? In order to answer that question, I performed the calculations described above for several γ's. The results (for $q = 1.0$) are presented in Fig. 11. We see that, as expected, inside the stellar disk a gas-layer immersed in a more massive stellar disk will be comparatively thinner. At large galactocentric radii the thickness of the gas layer becomes virtually independent of the $M/\mathcal{L}$ ratio of the stellar disk. The same conclusion can be reached from Fig. 5, where we see that, beyond the optical disk, the derived midplane mass densities for different $M/\mathcal{L}$ -disks are nearly equal.

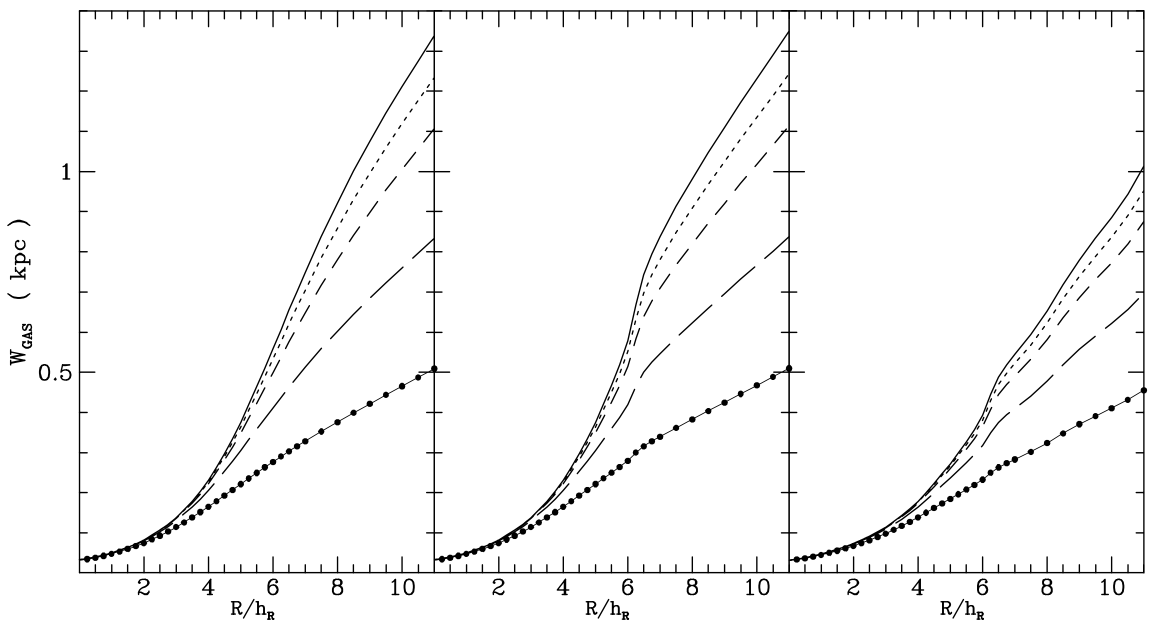

Fig. 10.— For a given rotation curve (BE89), I show how the thickness of the gas layer, W_{gas} [$\approx FWHM/2.35$, as defined by Eq. (5)], depends on the flattening of the DM halo ($q = c/a$). The different line-types/symbols correspond to different halo flattenings q ; $q = 1.0$ (full line), $q = 0.8$ (dotted line), $q = 0.6$ (short dashed line), $q = 0.3$ (long dashed line)), and $q = 0.1$ (filled circles). The model curves presented were calculated for a gaseous velocity dispersion of 7.5 km s^{-1}. The left-hand side figure was calculated using a double exponential stellar disk, which is replaced by a truncated stellar disk for the middle panel. For the right-hand side plot I included the truncation of the stellar disk as well as the self-gravity of the gas. For these particular mass models the gaseous self-gravity influences the model widths more strongly than the truncation of the stellar disk does.

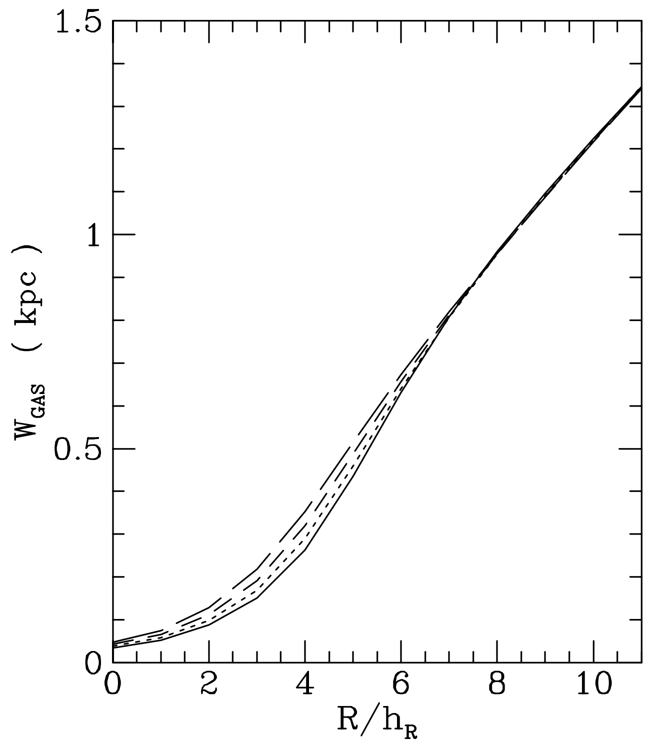

Fig. 11.— This figure shows how the thickness of the gas layer (W_{gas} [$\approx FWHM/2.35$, as defined by Eq. (5)]) depends on the mass-to-light ratio of the stellar disk for several galaxy models (truncated-stellar-disk+*round*-DM-halo) consistent with the observed properties of NGC 3198 (BE89). The different line types correspond to different mass-to-light ratios of the stellar disk ; ($M/\mathcal{L}$ =2.98, γ = 0.9) full line, ($M/\mathcal{L}$ =2.35, γ = 0.8) dotted line, ($M/\mathcal{L}$ =1.80, γ = 0.7) short dashed line, ($M/\mathcal{L}$ =1.32, $\gamma = 0.6$) long dashed line. Inside the optical disk, the extreme thinness of the H I disk (in absolute measures) will, quite likely, limit its usefulness for the determination of the $M/\mathcal{L}$ -ratio of the stellar disk to the nearest galaxies. Beyond the optical disk, the thickness of the gas layer becomes virtually independent of the mass-to-light-ratio of the stellar disk, so that a determination of the DM-halo flattening is independent of $M/\mathcal{L}$. As for Fig. 10 the model curves presented were calculated for a gaseous velocity dispersion of 7.5 km s^{-1}.

2.3.9. Effects of incomplete modelling

It is instructive to see how uncertainties in gaseous velocity dispersion and uncertainties in the derivation of the vertical force affect our estimates of the DM-halo flattening. Another point of interest is to investigate what differences may arise when using the local instead of the global approach.

To summarize the following sections: the errors introduced by using the Gaussian-equivalent method (typically a 10-30% too round halo) tend to cancel out those introduced by neglecting the self-gravity of the gas (20-60% too flat a halo).

2.3.10. Uncertainties in the velocity dispersion

In many practical situations it may be that measurements of the gaseous velocity dispersion are not available. This severely limits our ability to determine the flattening of the DM halo. In some face-on galaxies the azimuthally averaged gaseous velocity dispersion is observed to decline radially from around 12 km s^{-1} in the center to remain constant at 7 km s^{-1} beyond R_{25} (van der Kruit & Shostak 1982; Dickey *et al.* 1990). In other systems, the region beyond R_{25}, as well as the inter-arm regions appear to have a constant velocity dispersion of 7 km s^{-1}, while on the arms values around 13 km s^{-1} are reported, (Shostak & van der Kruit 1984; see Kamphuis 1993 for a review). In summary, the measurements to date indicate that the gaseous velocity dispersion beyond the optical disk has a value of around 7 km s^{-1}.

Overestimating the gaseous velocity dispersion by a factor of $(1 + x)$ causes an overestimate of the midplane mass density by a factor of $(1 + x)^2$. Beyond the optical disk, too flat a DM-halo distribution would be inferred (by the same factor $(1 + x)^2$).

2.3.11. Uncertainties in the vertical force

Here I estimate the effects of neglecting certain components to the vertical force (e.g. the self-gravity of the atomic gas, magnetic forces, or the gravitational force due to some remote point source). A mass-model which uses an underestimate of the true vertical force requires a larger DM density and thus a smaller values of the halo flattening to reproduce the observed gas layer widths. Thus, underestimating the vertical force by a factor $(1 + y)$ results in too small an estimate for the halo flattening (by a factor $[1 + y]$). The inverse is true when working with an overestimate of the vertical force.

Neglecting the self-gravity of the neutral atomic gas, which can typically contribute 30 % to the vertical force (Sec. 2.3.6. and Fig. 7), will result in a 30 % too small inferred halo flattening. Since the known molecular gas content of galaxies rarely exceeds 10% of the stellar mass (which contributes roughly 20% to K_{z} at large distances, see Sec. 2.3.2. and Fig. 6), and is confined to the inner parts of the galaxy like the stars, I expect that neglecting the molecular gas will result in an underestimate of q by at most 2%.

2.3.12. Using the Gaussian-equivalent method

Application of the Gaussian-equivalent method to an observed set of gas layer widths underestimates the inferred midplane density by a radially varying amount (see Sec. 2.3.2., and Fig. 5). As a result the inferred halos will be too round and have core radii that are too large.

2.4. DISCUSSION AND CONCLUSIONS

In the previous sections we have seen that a flattened dark halo imprints a very specific signature on the flaring of the gas-layer (Fig. 10). Measurement of this flaring allows for the determination of the DM-halo flattening.

Although the global approach is limited by some of the same assumptions as the local approach (isothermality of the gas, zero non-thermal pressure terms, constant $M/\mathcal{L}$ -ratio of the stellar disk, alignment between DM halo and stellar disk, ...), it treats some other aspects much better (radial gradients in stellar surface density, the effects of the rising rotation curve, the non-cylindrical symmetry of the potential, ...). In particular the region where the rotation curve rises sharply and the region where the stellar disk truncates are better analyzed using the global approach. In those parts where the rotation curve is 'flat' and which are not too close to the truncation of the stellar disk the Gaussian-equivalent and multi-component methods can be used to reasonable accuracy. However, the global approach is less sensitive to small scale irregularities (Fig. 9). To obtain reliable results, any applied method *must* include the self-gravity of the gas.

Therefore, I propose that the more robust global approach (Sec. 2.3.1.) should be used in programs aimed at determining the flattening of the dark matter halo. For a set of global mass distributions with varying halo flattening one can calculate the flaring behaviour of the gaseous disk. The DM-halo model exhibiting the best agreement between calculated and observed gas-layer widths then yields the halo flattening. The accuracy of the determined flattening can be gauged by varying the structural parameters of the individual mass components. Since the velocity dispersion of the gas is a crucial parameter in the analysis, care must be taken to determine its radial dependence. This will be done done in a forthcoming paper where I will analyze the flaring gas layer of thee almost edge-on galaxy NGC 4244.

2.4.1. Suitable systems

Nearby edge-on spiral galaxies with large (extending beyond the optical disk) neutral hydrogen envelopes are possible targets for studies of this kind. Symmetric systems are preferred since it is more likely that such systems are in equilibrium. Furthermore suitable systems should not exhibit strong warping. For systems with moderate warps, the kinematical information can be used to disentangle flaring from warping. Unfortunately these kind of systems might be rare.

In order to investigate the possibility of determining the thickness of the gas-layer in less inclined systems, I simulated H I observations of two models similar to NGC 3198 (inclined by 72° w.r.t. the line of sight). In the thin disk model, I constrained the gas-layer to have a FWHM of 100 pc everywhere, while in the flaring disk model the gas-layer has a vertical distribution calculated using the multi-component method (including the self-gravity of the gas, eqn. [42]). Both models were calculated with a gaseous velocity dispersion of 7.5 km s^{-1}. For a given set of observational parameters (15″ beam [→ 700 pc] and 2.56 km s^{-1} velocity resolution) I calculate the intensities originating from all points in the model galaxy for all velocities. Taking the normalized second moment with respect to radial velocity yields the apparent velocity dispersion for all points in the model galaxy. In Fig. 12 I present the two model velocity dispersion maps. The systematic differences, of the order of 5 km s^{-1}, arise due to the fact that a line of sight through a flaring disk samples a wider range in position angle and galactocentric radius than the line of sight through a thin disk. In principle, the gaseous velocity dispersion can be determined after the layer-thickness-effects are corrected for. The thickness of the gas layer can be derived by comparing individual channel maps[11]. Contour maps of a particular channel are presented in Fig. 13 : in the top panel the thin disk map is shown, the middle panel shows the thick disk equivalent while the difference between the two is contoured in the lower panel. Due to its larger vertical scale-height, the projected width of the thick-disk channel map should be larger than that of the thin-disk, while the average surface brightness will be reduced. This signature of the thick disk is easily recognized in the displayed contour maps. Furthermore, contrary to edge-on galaxies, the flaring can be measured in many different channel maps so that local irregularities (e.g. spiral streaming motions, bubbles, ...) are less likely to hamper the determination of the radial behaviour of the flaring (cf. Olling & van Gorkom, 1995).

Therefore I expect that it must be possible to experimentally determine both the gaseous velocity dispersion and the thickness of the gas-layer for moderately inclined systems as well.

2.4.2. A control sample

It might be possible to test the importance of neglected physics in galaxies where the rotation curve falls in Keplerian manner. In such systems the contribution of the dark matter to the global potential is presumably small, thereby eliminating the gas layer thickness dependence on the shape of the DM halo. As a result the thickness of the gas layer should depend on the total visible mass of the galaxy and the gaseous velocity dispersion only. Some galaxies exhibit falling rotation curves, albeit not in Keplerian manner (Casertano & van Gorkom 1991; Broeils 1992).

The measured width of the gas layer can then be compared with model predictions. If the gas layer is observed to be thicker than predicted, one might conclude that magnetic and cosmic ray pressures are important. On the other hand, a gas layer thinner than predicted

[11] A channel map is an image (of a galaxy) taken in a “narrow band filter” : 2.56 km s^{-1} wide in this case.

indicates that either the ionizing extra-galactic radiation field is important (e.g. Maloney 1993), or that an unseen disk-like DM component is present (i.e. the "clumpuscules" proposed by Pfenniger *et al.* 1994a, and Pfenniger & Combes 1994b).

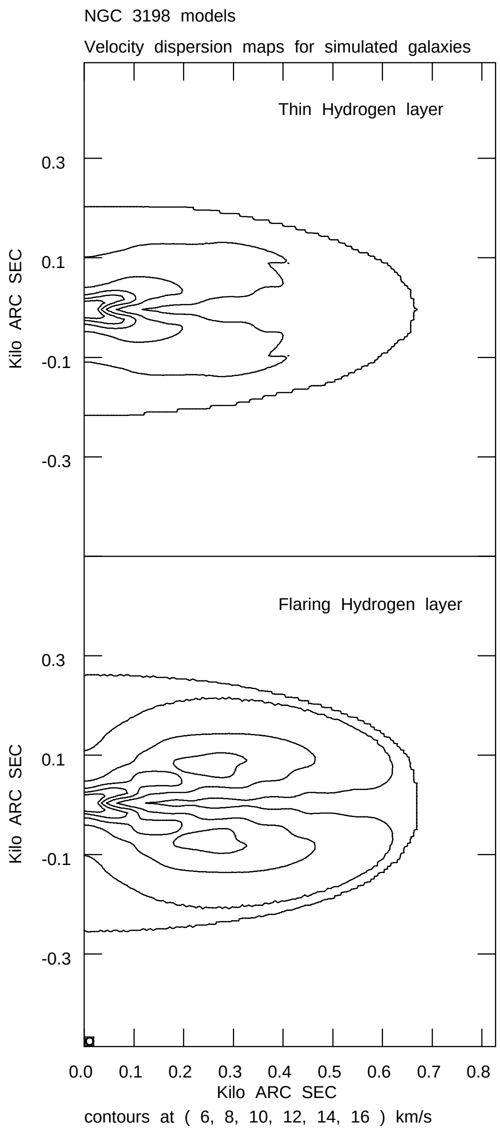

Fig. 12.— This figure illustrates one of the observable effects of a flaring H I -layer. The apparent gaseous velocity dispersion (i.e. the second moment w.r.t. recession velocity) of two galaxy models is shown here (the *input* dispersion was 7.5 km s^{-1}). The upper panel was calculated setting the $FWHM$ of the gas layer to 100 pc everywhere, while the lower panel corresponds to a model run where the vertical distribution of the H I layer was calculated in a self-consistent manner (cf. the procedure outlined in Appendix 2.7. for a model with $q = 1$). A flaring disk imprints a clearly different pattern on the apparent velocity dispersion map. Since this is a large-scale pattern, its detection should be relatively easy. The model calculations were convolved to a $15''$ x$15''$ beam, whereas the channels are square and 2.56 km s^{-1} wide. For both models I used the rotation curve and H I surface density distribution of NGC 3198 (BE89).

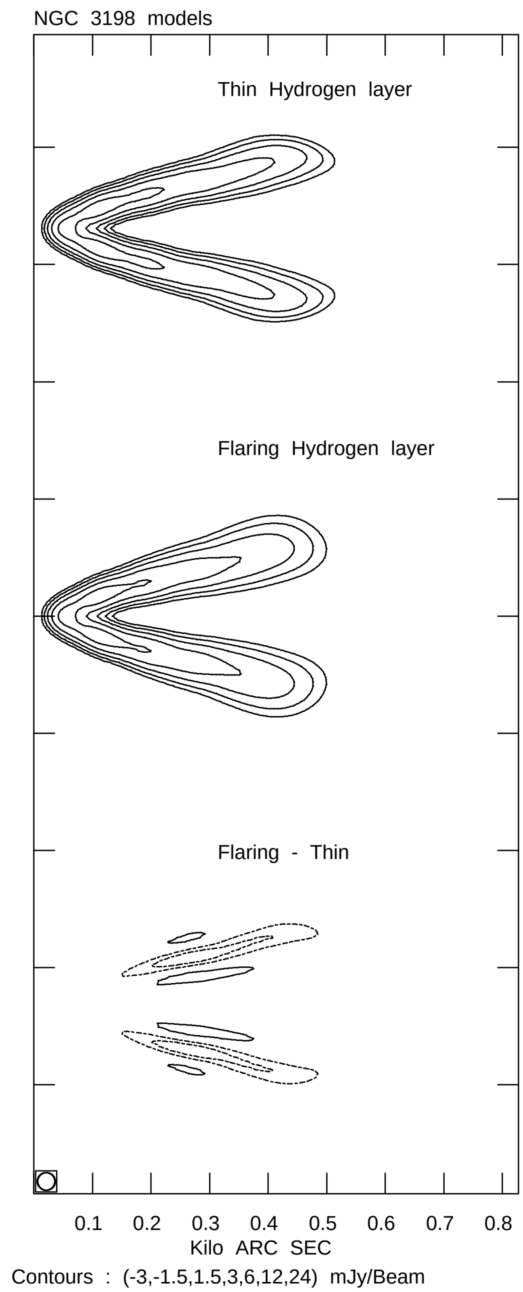

Fig. 13.— This figure shows that the effects of a flaring H I layer are also visible in individual channel maps. The top panel shows a channel map ($|V_{\rm sys} - V_{\rm chan}|= 104$ km s^{-1}, smoothed down to 30″ x30″) for the thin hydrogen disk described in Fig. 12. In the middle panel I show the same channel but now for the flaring-disk model. The "butterfly-wing" for the thin hydrogen layer model (upper panel) is clearly narrower and more peaked than its flaring equivalent (middle panel). Because the difference between the two models (lower panel) is significant over a large range in radii, it is expected that local irregularities (in the velocity field and/or the surface density distribution) will not be a limitation in determining the thickness of the hydrogen layer of inclined galaxies.

2.4.3. *Summary*

I have investigated the use of accurate determination of the thickness of the H I -layer in external galaxies. In combination with constraints set by the gaseous velocity dispersion and the rotation curve, I find that in principle it is possible to determine the shape of DM halos. The gaseous self-gravity contributes significantly to the vertical force field (up to 40%) but can be modeled accurately using the global approach (Sec. 2.3.1.) outlined in this paper. The thus determined halo flattening is independent of the particular choice of disk-halo decomposition.

In practice (not necessarily edge-on) systems with extended H I -disks and regular velocity fields should be used, provided that they are observed with high angular and velocity resolution.

I would like to thank Jacqueline van Gorkom for the support, encouragement and stimulating discussions during my years in graduate school. Michael Rupen's work initiated this line of research: the many discussions we had over the years and his comments on an earlier version of this paper were of great help to me. Furthermore I would like to thank HongSheng Zao who reminded me of quite a few analytic tricks applied in Appendix 2.7.. Penny Sackett helped me a lot by providing me with the relations for $K_{\rm z}$ and F_R of flattened DM halos. I want to thank Kevin Prendergast for his suggestion to investigate the global approach and his careful reading of an earlier version of the manuscript. David Schiminowich, as an un-prejudiced reader, provided useful tips for improvement. I also thank Phil Maloney, the referee, for some useful suggestions to improve this paper. And finally I would like to thank NRAO and the Kapteyn Astronomical Institute for developing and maintaining the AIPS and GIPSY software packages respectively.

This work was supported in part through an NFS grant (AST-90-23254 to J. van Gorkom) to Columbia University.

Appendices

2.5. APPENDIX-A: ROTATION CURVES OF FLATTENED DM-HALOS

As mentioned before, it is not possible to constrain the DM-halo flattening by measurements of the equatorial rotation curve since both round and flattened mass distributions can generate the same rotation curve. In this Appendix I show that the DM-halo model used by Sackett & Sparke (1990):

$$\rho_{\rm h}(R,z;q) \quad = \quad \rho_{\rm h,0}(q) \ \left(\frac{R_{\rm c}(q)^2}{R_{\rm c}(q)^2 + R^2 + (z/q)^2}\right) \ , \tag{15}$$

(where $R_{\rm c}$, $\rho_{\rm h,0}$ and q $(= c/a)$ are the DM-halo core radius, central density and flattening respectively) defines a one-parameter family of halo models with essentially the same equatorial rotation curve if core radius and central density depend in a specific way on this one parameter, q [Eqns. (22) and (23) respectively].

SRJF94 give a general relation for both the vertical and the radial force due to such a dark halo [their Eqn. (6)]. Evaluating this relation in the midplane, I find that the equatorial rotation curve arising from a flattened DM-halo is given by:

$$V^2_{\rm halo}(R; \rho_{\rm h,0}, R_{\rm c}, q) \;=\; V^2_{\rm halo}(\infty; \rho_{\rm h,0}, R_{\rm c}, q) \times Q(R; R_{\rm c}, q) \;, \tag{16}$$

with $\qquad Q(R; R_{\rm c}, q) \;=$

$$\left\{1 - \left(\frac{g(q)}{\arctan g(q)}\right) \left(\frac{q^2 {R_{\rm c}}^2(q)}{R^2 + (1-q^2){R_{\rm c}}^2(q)}\right) \arctan\left(\frac{R^2 + (1-q^2){R_{\rm c}}^2(q)}{q^2 {R_{\rm c}}^2(q)}\right)\right\} \;, \tag{17}$$

and $\qquad V^2_{\rm halo}(\infty; \rho_{\rm h,0}, R_{\rm c}, q) \;=\; 4\pi G\, \rho_{\rm h,0}(q)\, {R_{\rm c}}^2(q)\, f(q) \;,$ (18)

while $f(q)$ and $g(q)$ are given by:

$$f(q) = \left(\frac{q\;\arccos q}{\sqrt{1-q^2}}\right) \qquad\qquad g(q) = \left(\frac{\sqrt{1-q^2}}{q}\right) \;. \tag{19}$$

It is easily verified that Eqn. (16) indeed yields the familiar $V^2_{\rm h}(R) = V^2_{\rm h}(\infty)\,\{1 - (R_{\rm c}/R)\arctan(R/R_{\rm c})\}$, the rotation curve due to a round halo.

Changing the flattening of the halo should not change the halo rotation curve significantly, that is to say: $V^2_{\rm halo}(R; q) \approx V^2_{\rm halo}(R; 1)$ for all radii. Noting that $f(1) = 1.0$, I find that at infinity the following relation holds:

$$\rho_{\rm h,0}(1)\, {R_{\rm c}}^2(1) \;=\; \rho_{\rm h,0}(q)\, {R_{\rm c}}^2(q) \times f(q) \;. \tag{20}$$

Requiring that the round-halo rotation curve equals the flattened-halo rotation curve at $R = R_{\rm c}(q)$ leads to the following relation:

$$\left(1 \;-\; \frac{R_{\rm c}(1)}{R_{\rm c}(q)} \arctan\frac{R_{\rm c}(q)}{R_{\rm c}(1)}\right) \;=$$

$$\left\{1 - \left(\frac{g(q)}{\arctan g(q)}\right)\left(\frac{q^2}{2-q^2}\right) \arctan\left(\frac{2-q^2}{q^2}\right)\right\} \;. \tag{21}$$

Noting that the RHS of this equation varies between 1.28 and 1.00 for $q \in [0.1, 1.0]$, so that $R_c(q)/R_c(1)$ is constrained to the interval $[1.00, 1.242]$, I expand (to second order) the left-hand and right-hand sides of this equation with respect to $R_c(q)/R_c(1)$ and q respectively. The resulting quadratic equation is solved to obtain the core radius of the DM-halo as a function of flattening. The central density is then found from Eqn. (20). After substituting the solutions for $R_c(q)$ and $\rho_{h,0}(q)$ in the equation for the rotation curve [Eqn. (16)] it is found that the rotation curves of flattened DM-halos reproduce the rotation curve of a round halo to within 7 % (for q =0.2). This error is maximal for $R = 0$, changes sign at $R = R_c(q)$ and slowly drops from -2% at two core radii to 0% at infinity. Since these deviations are large in the region where rotation curves are determined, such accuracy is not acceptable for our purpose. A little experimentation leads to a solution which is more acceptable: our best approximation (errors $\leq 1.4\%$) to the dependence of halo core radius and central density on its flattening q is graphically presented in Fig. 2 and algebraically below:

$$\begin{aligned} R_c(q) &= R_c(1) \times \left(1.209 - 0.332q + 0.123q^2\right) \\ &= R_c(1) \times \mathcal{C}(q) \ , \end{aligned} \tag{22}$$

and
$$\begin{aligned} \rho_{h,0}(q) &= \rho_{h,0}(1) \times \left(\frac{1}{f(q)\mathcal{C}(q)^2}\right) \left(0.954 + 0.0533q - 0.0073q^2\right) \\ &= \rho_{h,0}(1) \times \mathcal{H}(q) \qquad \approx \qquad \left(\frac{\rho_{h,0}(1)}{q}\right) \ , \end{aligned} \tag{23}$$

where $\lim_{q\to 1} R_c(q) = R_c(1)$ and $\lim_{q\to 1} \rho_{h,0}(q) = \rho_{h,0}(1)$. Substituting (23), (22) and (19) into Eqn. (15), I find that at large distances the local DM-halo densities are roughly proportional to $1/f(q) \approx 1/q$.

2.6. APPENDIX-B: ON THE DISK-HALO CONSPIRACY

In order to calculate the potential of the galaxy, the mass distributions of both the stellar disk and the DM-halo need to be parameterized in a convenient way. In this section I describe how the DM-halo structural parameters are related to those of the stellar disk. Given the photometry of the stellar disk and the observed rotation curve, a disk-halo mass model is fully determined by *one* parameter which regulates the relative importance of stars and dark matter. Following Bottema (1993) I choose the parameter, γ, to be the fraction of the peak observed rotation curve which is due to the stellar disk [defined by Eq. (29)]. With such a parameterization of the disk-halo decomposition available, it is possible to investigate the effects of the stellar mass-to-light ratio upon the flaring of the gas layer. In accordance with van ABBS85 and LF89, I find that a wide range of stellar mass-to-light ratios (γ's) produce acceptable "fits" to observed rotation curves.

Since the light distribution of the stellar disk is relatively well known, the first step in tackling the disk-halo conspiracy is the description of the rotation curve due to the stellar disk. When assuming a constant mass-to-light ratio, the stellar density distribution can be described, to first order, as radially exponential and vertically thin. The amplitude of the rotation curve due to such a thin exponential stellar disk depends only on its central surface density and radial scale length. The *shape* is fully determined by the radial density distribution. Casertano (1983) has shown that both the amplitude and shape of stellar rotation curves are sensitive to the thickness of the stellar disk as well as to the truncation radius, $R_{\rm max}$ (vdKS81a&b; vdKS82a&b; BD93). Therefore, the disk-halo conspiracy too will vary with the details of the stellar mass distribution. While the amplitude of the inner stellar rotation curve depends rather strongly on the thickness of the stellar disk, the outer rotation curve is virtually independent thereof. I will now investigate the dependence of the stellar rotation curve on the structural parameters of the stellar disk ($h_{\rm R}$, $R_{\rm max}$, and $z_{\rm e}$).

I calculated stellar rotation curves, using the program ROTMOD in GIPSY (van der Hulst *et al.* 1992), for several truncation radii and disk thicknesses, and vertical distributions. As it turned out, the rotation curves of such stellar disks can be parameterized by a rotation speed at an inner ($R_{\rm inn}$) and an outer ($R_{\rm out} = \; x \; R_{\rm inn}$) radius:

$$V^2_{\rm rot,stars}(R_{\rm inn}) \;\; = \;\; f_{\rm m} \; \pi \; G \; h_{\rm R} \; L(0) \; M/\mathcal{L} \qquad (24)$$

$$V_{\rm rot,stars}(R_{\rm out}) \;\; = \;\; f_{\rm x} \; V_{\rm rot,stars}(R_{\rm inn}) \; , \qquad (25)$$

where $L(0)$ is the central surface brightness, $M/\mathcal{L}$ the mass-to-light ratio, and $h_{\rm R}$ the radial scale length of the stellar disk. I take $R_{\rm inn} = 2.3h_{\rm R}$, because a typical stellar disk (truncated at $4.5h_{\rm R}$ and $h_{\rm R}/z_{\rm e}$=0.1) has its maximum rotation speed at this distance. The constants $f_{\rm m}$ and $f_{\rm x}$ depend upon the the vertical distribution and the radial truncation of the stellar disk. For the outer radius I used three different values, $6.0h_{\rm R}$, $8.0h_{\rm R}$ and $10.0h_{\rm R}$. The results are presented in Table 1 for a range in parameters covering the observed range in thickness and truncation radius (vdKS81a&b; vdKS82a&b; Bottema *et al.* 1987; BD93).

The listed values are the average of the rotation curves for a vertically exponential and a vertically sech^2 stellar disk. With this choice for the two vertical distributions, sech-squared and exponential, I bracket the suggested range of suggested distributions (van der Kruit, 1988). The uncertainty concerning the true vertical distribution translates directly into uncertainties,Δf, in $f_{\rm m}$ and $f_{\rm x}$. Experimentally I find, $\Delta f_{\rm m} \approx (2\Delta f_6) \approx (2\Delta f_8) \approx (2\Delta f_{10}) =$ 0.6%, 1.2%, 1.7% and 2.3% for $z_{\rm e}/h_{\rm R}$= 0.05, 0.10, 0.15 and 0.20 respectively), so that $f^{\rm exp} = f + \Delta f$ and $f^{\rm sech2} = f - \Delta f$. Thus, if the structural parameters of the stellar disk are well known the errors on the f-values are small. In situations where the thickness of the stellar disk is not known (as for all non edge-on systems) one must use the average values, $\overline{f_{\rm m}}$ and $\overline{f_{\rm x}}$, which are listed in the columns labeled "$z_{\rm e}/h_{\rm R}$ = *averaged*". The uncertainties on these averages are typically 4.5, 2.0, 2.0 and 2.0 %. If also no information is available on the location of the truncation radius, then $f_{\rm m}$ f_6, f_8, and f_{10} should be representative of the range in allowed values: I suggest $f_{\rm m}$= $0.73 \pm 6\%$, $f_6 = 0.68 \pm 10\%$, $f_8 = 0.57 \pm 10\%$ and $f_{10} = 0.50 \pm 10\%$.

2.6.1. The Mass-to-Light Ratio of the Stellar Disk

Now I turn to the dark halo contribution to the observed rotation curve. As usual, the (square of the) observed rotation curve is generated by the quadratic sum of the constituting mass components:

$$V^2_{\rm rot,obs}(R) \;=\; V^2_{\rm rot,stars}(R) \;+\; V^2_{\rm rot,bulge}(R) \;+\; V^2_{\rm rot,gas}(R) \;+\; V^2_{\rm rot,halo}(R)\;. \qquad (26)$$

Now I define the gas-bulge-corrected observed rotation speed as the square root of (27).

$$\mathcal{V}^2_{\rm rot,obs}(R) \;=\; V^2_{\rm rot,obs}(R) - V^2_{\rm rot,bulge}(R) - V^2_{\rm rot,gas}(R)\;, \qquad (27)$$

$$\text{so that :}\qquad \mathcal{V}^2_{\rm rot,obs}(R) \;=\; V^2_{\rm rot,stars}(R) \;+\; V^2_{\rm rot,halo}(R)\;. \qquad (28)$$

Furthermore I define γ and $\beta_{\rm x}$ (= the slope of the rotation curve) :

$$\gamma \;=\; \frac{V_{\rm rot,stars}(2.3h_{\rm R})}{\mathcal{V}_{\rm rot,obs}(2.3h_{\rm R})} \qquad\qquad \beta_x \;=\; \frac{\mathcal{V}_{\rm obs}(x\; h_{\rm R})}{\mathcal{V}_{\rm obs}(2.3h_{\rm R})}\;. \qquad (29)$$

Given the observed radial scale length and central surface brightness of the stellar disk, the mass-to-light-ratio is a function of the stellar contribution to the peak rotation curve (γ) only and is given by [from Eqns. (24) and (29)]:

$$M/\mathcal{L}\;(\gamma) \;=\; \left(\frac{\mathcal{V}^2_{\rm obs}(2.3h_{\rm R})}{f_{\rm m}\;\pi G\; h_{\rm R}\; L(0)}\right)\times\gamma^2 \;=\; 10.25\left(\frac{\mathcal{V}^2_{\rm obs,100}(2.3h_{\rm R})}{f_{\rm m,0.722}h_{\rm R,1}L_{100}(0)}\right)\times\gamma^2\;, \qquad (30)$$

where $\mathcal{V}_{\rm obs,100}(2.3h_{\rm R})$ is the gas-bulge-corrected observed rotation speed at 2.3 radial scale-lengths in units of 100 km s^{-1}, $L_{100}(0)$ is the central surface brightness of the stellar disk in units of 100 $L_\odot/{\rm pc}^2$, $h_{\rm R,1}$ is the radial scale-length in units of 1 kpc and $f_{\rm m,0.722}$ in units of 0.722 (the $f_{\rm m}$-value appropriate for a typical stellar disk with $h_{\rm R}/z_{\rm e}$= 10.0 and $R_{\rm max}/h_{\rm R}$= 4.5).

2.6.2. The Core Radius of the DM halo

For a given observed rotation curve and a calculated stellar rotation curve *shape*, the core radius is determined uniquely by γ. Applying Eqn. (28) at 2.3 and $x\ h_{\rm R}$, eliminating the terms depending on the stellar rotation curve, and using Eqn. (16) with $q = 1$, I find that the following relations hold:

$$\left(\frac{(\beta^2_{\rm x} - (f_{\rm x}\;\gamma)^2)}{1-\gamma^2}\right) \;=\; \left(\frac{V^2_{\rm rot,halo}(x\; h_{\rm R})}{V^2_{\rm rot,halo}(2.3h_{\rm R})}\right) \;\approx\; a_{\rm x,0} + a_{\rm x,1}\left(\frac{R_{\rm c}}{h_{\rm R}}\right) + a_{\rm x,2}\left(\frac{R_{\rm c}}{h_{\rm R}}\right)^2\;. \qquad (31)$$

The approximation (31) is valid for small ranges in $R_{\rm c}/h_{\rm R}$ only. I list these ranges, together with the ranges for the left-hand side of (31) and the appropriate $a_{\rm x}$-values in Table 2. These piecewise approximations recover the right-hand side of Eqn. (31) to within 0.2 %. No effort has been made to match the pieces smoothly.

For any assumed γ and measured β_{x} and f_{x} one can calculate the left-hand side of Eqn. (31) and find the appropriate a_{x}-values in Table 2 from which $\mathcal{R}_c = R_{\mathrm{c}}/h_{\mathrm{R}}$ follows:

$$\left(\frac{R_{\mathrm{c}}}{h_{\mathrm{R}}}\right)(\gamma;\beta_x,f_{\mathrm{x}}) \;\approx\; \frac{\left(-a_{\mathrm{x},1}+\sqrt{(a_{\mathrm{x},1})^2-4a_{\mathrm{x},2}(a_{\mathrm{x},0}-lhs_{\mathrm{x}})}\right)}{2a_{\mathrm{x},2}} \;\equiv\; \mathcal{R}_c(\gamma)\ . \tag{32}$$

Table 1: Coefficients for stellar rotation curves

$\frac{R_{\rm max}}{h_{\rm R}}$	$z_{\rm e}/h_{\rm R} = 0.05$				$z_{\rm e}/h_{\rm R} = 0.10$			
	$f_{\rm m}$	f_6	f_8	f_{10}	$f_{\rm m}$	f_6	f_8	f_{10}
2.0	0.807	0.516	0.443	0.395	0.798	0.518	0.445	0.397
2.5	0.841	0.553	0.473	0.421	0.809	0.563	0.482	0.429
3.0	0.774	0.612	0.522	0.464	0.748	0.623	0.531	0.472
3.5	0.756	0.647	0.549	0.487	0.731	0.658	0.559	0.496
4.0	0.750	0.670	0.567	0.502	0.724	0.682	0.576	0.511
4.5	0.747	0.688	0.578	0.511	0.722	0.700	0.588	0.520
5.0	0.746	0.703	0.587	0.518	0.720	0.714	0.597	0.527
5.5	0.746	0.718	0.592	0.522	0.720	0.729	0.603	0.532
6.0	0.745	0.734	0.597	0.525	0.720	0.743	0.607	0.535
6.5	0.745	0.724	0.600	0.528	0.719	0.735	0.611	0.537
7.0	0.745	0.722	0.603	0.529	0.719	0.733	0.614	0.538
∞	0.745	0.721	0.607	0.534	0.719	0.732	0.617	0.543

Table 1: , continued

$\frac{R_{\rm max}}{h_{\rm R}}$	$z_{\rm e}/h_{\rm R} = 0.15$			
	$f_{\rm m}$	f_6	f_8	f_{10}
2.0	0.767	0.528	0.454	0.405
2.5	0.778	0.574	0.492	0.438
3.0	0.722	0.633	0.540	0.480
3.5	0.706	0.668	0.568	0.504
4.0	0.700	0.693	0.586	0.519
4.5	0.697	0.711	0.598	0.529
5.0	0.696	0.726	0.607	0.536
5.5	0.695	0.740	0.613	0.541
6.0	0.695	0.753	0.617	0.544
6.5	0.695	0.745	0.621	0.546
7.0	0.695	0.743	0.624	0.548
∞	0.695	0.742	0.627	0.552

Table 1: , continued

$\frac{R_{max}}{h_R}$	$z_e/h_R = 0.20$				$z_e/h_R = averaged$			
	f_m	f_6	f_8	f_{10}	$\overline{f_m}$	$\overline{f_6}$	$\overline{f_8}$	$\overline{f_{10}}$
2.0	0.748	0.534	0.460	0.410	0.780	0.524	0.451	0.402
2.5	0.749	0.584	0.501	0.446	0.794	0.569	0.487	0.434
3.0	0.698	0.643	0.549	0.488	0.736	0.628	0.536	0.476
3.5	0.683	0.679	0.577	0.513	0.719	0.663	0.563	0.450
4.0	0.677	0.703	0.596	0.528	0.713	0.687	0.581	0.515
4.5	0.674	0.722	0.608	0.538	0.710	0.705	0.593	0.525
5.0	0.673	0.737	0.617	0.545	0.709	0.720	0.602	0.532
5.5	0.672	0.751	0.623	0.550	0.708	0.735	0.608	0.536
6.0	0.672	0.762	0.628	0.553	0.708	0.748	0.612	0.539
6.5	0.672	0.755	0.631	0.555	0.708	0.740	0.616	0.542
7.0	0.672	0.754	0.634	0.557	0.708	0.736	0.619	0.543
∞	0.672	0.752	0.637	0.561	0.708	0.737	0.622	0.548

Table 2: Coefficients for the DM-halo core radius

lhs-range of (31)	$a_{6,0}$	$a_{6,1}$	$a_{6,2}$	R_c/h_R-range
$\in$ (1.00,1.90]	1.000	0.4300	0.1140	$\in$ (0 , 1.5]
$\in$ (1.90,3.04]	0.7363	0.7734	-0.001442	$\in$ (1.5, 3]
$\in$ (3.04,4.76]	0.2709	1.097	-0.05814	$\in$ (3 , 6]
$\in$ (4.76,5.81]	1.400	0.7439	-0.03038	$\in$ (6 ,10]
lhs-range of (31)	$a_{8,0}$	$a_{8,1}$	$a_{8,2}$	R_c/h_R-range
$\in$ (1.00, 2.10]	1.000	0.4884	0.1645	$\in$ (0 , 1.5]
$\in$ (2.10, 3.71]	0.7252	0.8293	0.05622	$\in$ (1.5, 3]
$\in$ (3.71, 6.76]	-0.3281	1.506	-0.05400	$\in$ (3 , 6]
$\in$ (6.76, 9.16]	-0.01879	1.4511	-0.05341	$\in$ (6 ,10]
lhs-range of (31)	$a_{10,0}$	$a_{10,1}$	$a_{10,2}$	R_c/h_R-range
$\in$ (1.00, 2.23]	1.000	0.5209	0.2007	$\in$ (0 , 1.5]
$\in$ (2.23, 4.20]	0.7508	0.8190	0.1103	$\in$ (1.5, 3]
$\in$ (4.20, 8.47]	-0.6623	1.702	-0.02960	$\in$ (3 , 6]
$\in$ (8.47,12.55]	-1.696	2.100	-0.06758	$\in$ (6 ,10]

2.6.3. The Central Density of the DM halo

The DM-halo central density is calculated from (28), (29) and (32). With

$$\mathcal{V}^2_{\rm obs}(2.3h_{\rm R}) \;=\; \gamma^2\mathcal{V}^2_{\rm obs}(2.3h_{\rm R}) + V^2_{\rm halo}(2.3h_{\rm R}) \;=\; \left(\frac{1}{1-\gamma^2}\right) V^2_{\rm halo}(2.3h_{\rm R}) \,,$$

it follows that

$$\rho_{\rm h,0}(\gamma;\beta_{\rm x},f_{\rm x}) \;=\; (0.185\; M_\odot\,{\rm pc}^{-3}) \left(\frac{\mathcal{V}_{\rm obs,100}(2.3h_{\rm R})}{h_{\rm R,1}}\right)^2 \times$$

$$\left\{\frac{(1-\gamma^2)}{\mathcal{R}_c(\gamma)^2}\right\} \left\{1-\left(\frac{\mathcal{R}_c(\gamma)}{2.3}\right)\arctan\left(\frac{2.3}{\mathcal{R}_c(\gamma)}\right)\right\}^{-1} \,, \tag{33}$$

where $\mathcal{R}_c$, the normalized core radius of the DM-halo, depends strongly upon the choice for γ, and only weekly upon the shape of the rotation curve (via $\beta_{\rm x}$) and the shape of the stellar mass distribution (via $f_{\rm x}$).

As an example I present the dependence of the mass-to-light ratio of the stellar disk (lower right panel of Fig. 3), the central density (upper left panel) and core radius (lower right panel) of the DM-halo on γ for NGC 3198 (photometry and rotation curve taken from BE89). The error-bars were calculated assuming the most common observational status : the truncation radius of the stellar disk is known but the thickness of the stellar disk is not. In this case, the accuracy with which one can determine the mass-to-light ratio of the stellar disk and the central density and core radius of the DM-halo are typically 3, 0.5 and 4 % respectively. If the thickness of the stellar disk is also known (as would be the case for edge-on galaxies), the errors decrease substantially, while they blow up (3.5%, 2.5%, and 20%, respectively) if neither the truncation radius nor thickness of the stellar disk are known. For galaxies which are about "maximum-disk", and have more or less flat rotation curves, Fig. 3 shows that the core radius of the DM-halo will be 7 ± (a factor of two) times the radial scale-length of the stellar disk, not too different from the maximum-disk-fits performed on real galaxies (Broeils 1992). Note that while the core radius of the dark halo approaches infinity as γ nears unity , the dark to luminous mass (upper right panel) is not singular.

I tested the procedure outlined above on simulated data, where I added (in quadrature) a stellar and a DM-halo rotation curve to represent a simulated total rotation curve. For falling, flat, as well as for rising simulated total rotation curves I was able to accurately recover the input parameters, provided that the slope of the total rotation curve is determined over as large a range in radius as possible.

As already pointed out by ABBS85 and LF89, mass models with a range (a factor of ten in some cases) in stellar mass-to-light ratios are consistent with observed rotation curves. I find, attempting to fit model rotation curves with "faulty" γ values (or $M/\mathcal{L}$ -ratios) that a wide range of stellar mass-to-light ratios is possible if small (≈ 2 %) differences between input and recovered rotation curves are allowed to occur. The differences between input and recovered rotation curves increase significantly inside the inner point and beyond the outer point which were used for to determine the slope of the rotation curve. This is illustrated in Fig. 4 where I show the resultant fits to the observed rotation curve of NGC3198 (BE89) for several γ's. I took the outer radius at 10 radial scale lengths. Although all γ values between 0.90 and 0.50 produce similarly acceptable fits, the low-γ-disks proposed by Bottema (1993) "fit" somewhat better. Since the velocity field of the inner parts of NGC 3198 deviates from circular rotation (Corradi *et al.* , 1991), the discrepancies between observed and model curves (in the inner parts) can not be used as an indication of goodness of fit.

Thus the method presented above presents us with an easy way to analyse many possible disk-halo decompositions. To obtain the core radius and central density of a flattened dark halo, one uses the Eqns. (32) and (33) and multiplies these values by $\mathcal{C}(q)$ [Eqn. (22)] and $\mathcal{H}(q)$ [Eqn. (23)] respectively.

2.6.4. The Edge of the Optical Disk

Combining the relations for the $M/\mathcal{L}$ -ratio, the DM-halo core radius and central density it follows that:

$$\frac{\rho_{\rm stars}(r)}{\rho_{\rm h}(r)} = 27.7\left(\frac{h_{\rm R}/z_{\rm e}}{10}\right)\left(\frac{0.722}{f_{\rm m}}\right)\left(\frac{\gamma^2}{1-\gamma^2}\right)\times$$

$$e^{-{\rm r}}\times\left\{\left(\mathcal{R}_c(\gamma)^2+r^2\right)\left[1-\left(\frac{\mathcal{R}_c(\gamma)}{2.3}\right)\arctan\left(\frac{2.3}{\mathcal{R}_c(\gamma)}\right)\right]\right\}\ , \qquad (34)$$

where $r = R/h_{\rm R}$. Thus the ratio of stellar to DM midplane densities is independent of the *amplitude* of the observed rotation curve and depends only weakly on the *shape* of the rotation curve (via $\beta_{\rm x}$), the truncation radius and thickness of the stellar disk (via $f_{\rm m}$ and $f_{\rm x}$ and $h_{\rm R}/z_{\rm e}$). The dependence of $\rho_{\rm stars}(r)/\rho_{\rm h}(r)$ upon galactocentric radius is graphically presented in Fig. 14 for several γ values (full line γ=0.9, dotted line $\gamma = 0.8$, short dashed line $\gamma = 0.7$, long dashed line $\gamma = 0.6$, dash-dotted line $\gamma = 0.5$). I term the distance at which the disk densities no longer dominates[12] the total midplane densities, $R_{\rm dde}$. The maximum-disk like models have $R_{\rm dde}$ values ranging from four to seven, corresponding to the range where some stellar disks are observed to be truncated (vdKS81a&b; vdKS82a&b). Furthermore we notice that the luminous-to-dark matter ratio decreases rapidly with decreasing γ and q values.

Recently Barteldrees & Dettmar (1993) have found that some spirals have edges in their light distribution as close in as two radial scale-lengths. Only for substantially rising rotation

[12] i.e. become smaller than a few times the DM density.

curves (say $\beta \geq 1.3$) and/or small γ values does $R_{\rm dde}$ become as small as two, suggesting that these systems have rising rotation curves and/or are DM dominated.

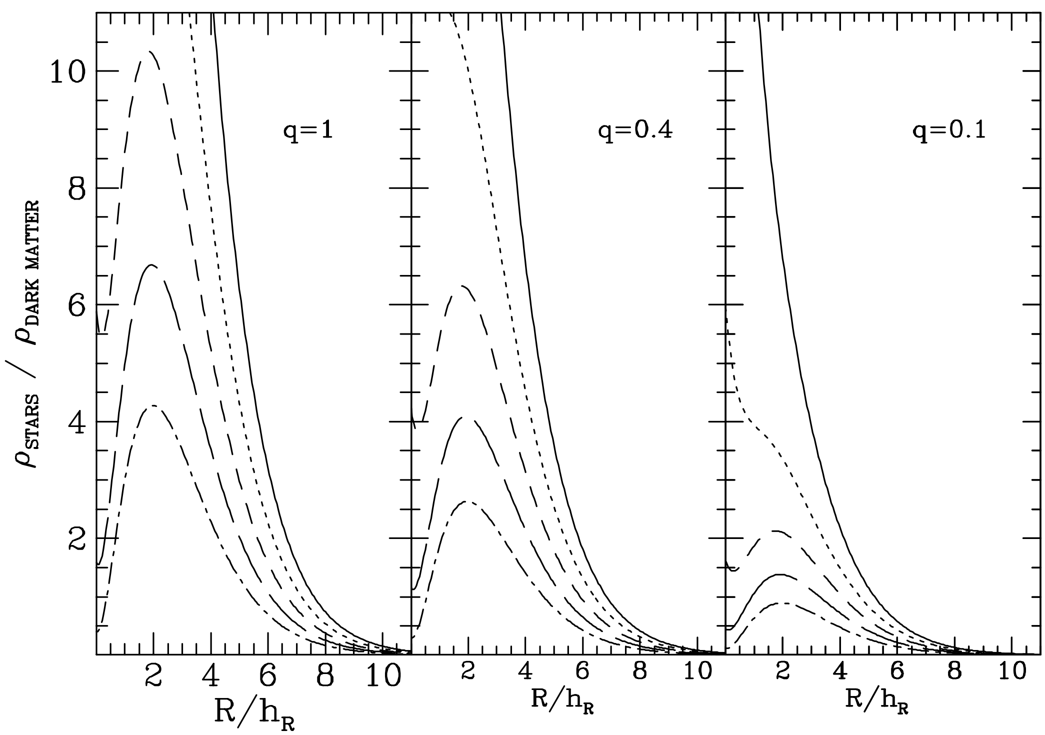

Fig. 14.— In this figure I present the radial dependence of the ratio of stellar to dark matter midplane density for several γ values (full line γ = 0.9, dotted line γ = 0.8, short dashed line γ = 0.7, long dashed line γ = 0.6, dash-dotted line γ = 0.5). The left most figure corresponds to a round DM halo (q=1.0), the right most to a very flattened DM halo (q=0.1) and the figure in the middle was calculated for a DM halo of intermediate flattening (q=0.4). This ratio is calculated using the disk-halo decomposition for a flat rotation curve presented in Appendix 2.6. , Eqn. (34). It can be clearly seen that in maximum-disk like models the stellar density dominates the midplane mass density out to about four radial scale-lengths, beyond which the contribution of the stellar density decreases sharply. For the low γ-models, the stellar density never really dominates.

2.7. APPENDIX-C: A SELF-CONSISTENT SOLUTION FOR THE MULTI-COMPONENT METHOD

In this Appendix, from the equation of hydrostatic equilibrium (12), I derive a self-consistent analytical solution for the vertical distribution of the gas for the multi-component method proposed by Bahcall (1984). The solution [Eqn. (42)] is in the form of an integral equation for $z(\rho_{\rm gas})$, which may be inverted numerically to yield $\rho_{\rm gas}(z)$. This equation can be used, in an iterative manner, to determine the local dark matter density. The model galaxies presented in Figs. 8, 12 and 13 were calculated using this analytic method. As it turns out, an analytic solution can be found if one makes the approximation that the DM-halo density is constant with height above the plane in the region where the gas is co-spatial with the DM-halo. For DM-halos which are not too flattened this is not a bad approximation for most galactocentric radii. For the gas as well as for the stars the following equation holds:

$$\sigma^2_{\rm z,i}\,\frac{d\;\ln\rho_i(z)}{d\;z} \;=\; -4\pi G\int_0^{\rm z}\{\rho_{\rm gas}(z')+\rho_{\rm stars}(z')+(\rho_{\rm halo}+\rho_{\rm rot})\}\;dz'\;. \tag{35}$$

The density and dispersion (ρ_i and $\sigma^2_{\rm z,i}$) can represent any isothermal component i, stars or gas. Since the right hand side of (35) is the same for stars and gas, it follows that the vertical distributions are powers of each other. The density distribution has to be normalized such that the integral equals the surface density. So I write:

$$\rho_{\rm gas}(z) \;=\; C_g\;(\rho_{\rm stars})^{p_{\rm sg}} = \rho_{\rm gas}(0)\left(\frac{\rho_{\rm stars}(z)}{\rho_{\rm stars}(0)}\right)^{p_{\rm sg}}\;, \tag{36}$$

$$\text{with}\quad p_{\rm sg} \;=\; \frac{\sigma^2_{\rm stars}}{\sigma^2_{\rm gas}}\qquad\text{and } C_g \text{ such that}\qquad \Sigma_{\rm gas}=\int_{-\infty}^{+\infty}\rho_{\rm gas}(z')\;dz'\;.$$

Similar relations can be defined for $\rho_{\rm stars}$. Differentiating (35) with respect to z yields:

$$A_{\rm gas}\,\frac{d^2\;\ln\rho_{\rm gas}(z)}{d\;z^2} \;=\; \rho_{\rm gas}(z)+\rho_{\rm stars}(z)+(\rho_{\rm halo}+\rho_{\rm rot})\;, \tag{37}$$

$$\text{with}\qquad A_{\rm gas} \;=\; -\frac{\sigma^2_{\rm z,gas}}{4\pi G}\;. \tag{38}$$

Solving for the gaseous component after defining $\alpha(z)=\ln\rho_{\rm gas}(z)$ I rewrite (37):

$$A_{\rm gas}\,\frac{d^2\;\alpha(z)}{d\;z^2} \;=\; e^\alpha + C_s\,(e^\alpha)^{p_{\rm gs}} + (\rho_{\rm halo}+\rho_{\rm rot})\;. \tag{39}$$